Spectral properties of a time-periodic Fokker-Planck equation

P. Alpatov and L. E. Reichl
Center for Statistical Mechanics and Complex Systems, University of Texas at Austin, Austin, Texas 78712
(Received 4 October 1993)

The Floquet spectrum of the time-periodic Fokker-Planck equation for a driven Brownian rotor is studied. We show that the Fokker-Planck equation can be transformed to a Schrödinger-like equation, with the same set of eigenvalues, whose dynamics is governed by a time-periodic Hamiltonian in which the diffusion coefficient plays a role analogous to Planck's constant. For a small diffusion coefficient, numerical calculations of the spectrum starting from the Schrödinger-like equation are more convergent than those starting from the Fokker-Planck equation. When the Hamiltonian exhibits a transition to chaos, those decay rates affected by the chaotic regime exhibit level repulsion. This level repulsion of decay rates, in turn, changes the behavior of a typical mean first passage time in the problem. The size of the diffusion coefficient determines the extent to which the stochastic dynamics is affected by the transition to chaos in the underlying Hamiltonian.

PACS number(s): 05.40.+j, 02.50.−r, 05.45.+b

I. INTRODUCTION

In a recent paper, Millonas and Reichl [1] studied the Brownian motion of a particle in a two-dimensional quartic potential well in the presence of white noise and strong friction. They showed that the dynamics of the Fokker-Planck equation governing this system is equivalent to that of a quantum system governed by a Hamiltonian in which a particle moves in a sixth-order potential well. The diffusion constant in the stochastic system plays the role of Planck's constant in the quantum system and also affects the shape of the potential well in the quantum system. The energy eigenvalues of the quantum system are the decay rates of the stochastic system. The Hamiltonian exhibits a transition to chaos and, when this happens, the energy-level nearest-neighbor spacing statistics changes from Poisson to Wigner-like, as one would expect in a quantum system which exhibits the manifestations of chaos [2]. However, since the Hamiltonian system is equivalent to the stochastic system, the Fokker-Planck equation is also affected by the transition to chaos. When the transition occurs, the decay rates of the Fokker-Planck equation exhibit level repulsion and the distribution of probability for the Brownian particle is shifted. This change in the behavior of the Fokker-Planck equation is *the stochastic manifestation of chaos.*

In this paper, we shall show that a similar analysis is possible for Brownian motion in which a time-periodic force acts on the Brownian particle. We will consider a one-dimensional Brownian rotor in the presence of a time and angle periodic force and in the presence of white noise and strong friction. A similar problem has been considered by Reichl, Chen, and Millonas [3,4] in which they study the statistics of the Floquet spectrum of the Fokker-Planck equation for such a periodically driven Brownian rotor, and by Chen [5] in which he studies the dynamical behavior of the Langevin equation for exactly the problem we consider here. Reichl, Chen, and Millonas have shown that there is a difference in the spectral spacing statistics of the Floquet eigenvalues for an integrable and a nonintegrable time-periodic Fokker-Planck equation. For the nonintegrable Fokker-Planck equation there was a transition in the spectral spacing statistics, as parameters were varied, which coincided with a change in a first passage time for the rotor. Chen showed that a qualitative change in the dynamics of the Langevin equation occurs in this same parameter range. None of the above papers attempted to connect the change in the dynamics of the Fokker-Planck equation to a transition to chaos in an underlying Hamiltonian system. The purpose of the present paper is to show that there is a Hamiltonian system underlying the dynamics of the time-periodic Fokker-Planck equation, and that by transforming to the Hamiltonian picture one can significantly improve the accuracy of numerical calculations of the Floquet spectrum for the system.

We begin in Sec. II by introducing the model for the periodically driven Brownian rotor and writing the Fokker-Planck equation for it. We also transform the Fokker-Planck equation to a Schrödinger-like form, using a transformation which preserves the Floquet spectrum and we compare the numerical results for the spectrum obtained from the Fokker-Planck equation and from the Schrödinger-like equation. The Schrödinger-like equation allows us to identify the Hamiltonian which governs the dynamics of this stochastic system. In Sec. III, we explore the properties of the Hamiltonian both classically and quantum mechanically. We find that the Hamiltonian undergoes a transition to chaos locally as parameters are varied. This transition leads to significant level repulsion in the Floquet eigenvalues of the quantum system governed by this Hamiltonian. In Sec. IV we return to the Schrödinger-like equation and show the transition to chaos in the Hamiltonian leads to level repulsion in those decay rates affected by the chaotic regime. This, in turn, strongly affects a typical mean first passage time for this system if the diffusion coefficient is sufficiently small. Finally, in Sec. V we make some concluding remarks.

II. MODEL

We will consider a model similar to the one described in [3–5] of the periodically driven Brownian rotor in a very viscous fluid. The motion of the rotor is constrained to the x-y plane. Its dynamics is effectively described by a one-dimensional Langevin equation

$$\gamma\frac{d\theta}{d\tau}=\epsilon'\sin(\omega\tau)\sin(\theta)+F_{\text{rand}}(\tau)\ , \tag{2.1}$$

where θ is the angular position of the rotor in the x-y plane, τ is the time, γ is the friction, ϵ' is the amplitude of the external torque, ω is the frequency of the external torque, and $F_{\text{rand}}(\tau)$ is a random external torque. The random torque is assumed to have a zero average, $\langle F_{\text{rand}}(\tau)\rangle=0$ and is δ correlated, $\langle F_{\text{rand}}(\tau)F_{\text{rand}}(\tau)\rangle=D\delta(\tau-\tau')$, where D is the diffusion coefficient. In Eq. (2.1) we have neglected the inertial effects because of the assumed large viscosity (and therefore large friction) of the fluid. The angular momentum of the rotor relaxes to equilibrium on a time scale much smaller than the period of the driving field and on a time scale much smaller than required for the rotor to relax to equilibrium in space.

Let us now make a transition to dimensionless variables $\epsilon=\epsilon'/\omega\gamma$, $t=\omega\tau$, and $F_{\text{rand}}(\tau)/(\omega\gamma)=\sqrt{g}\,\xi(t)$, where $g=D/\gamma^2\omega$ is a dimensionless diffusion coefficient and $\xi(t)$ is a dimensionless δ-correlated random torque. The Langevin equation now has the form

$$\frac{d\theta}{dt}=\epsilon\sin(t)\sin(\theta)+\sqrt{g}\,\xi(t)\ , \tag{2.2}$$

such that $\langle\xi(t)\rangle=0$ and $\langle\xi(t)\xi(t')\rangle=\delta(t-t')$, ϵ is the dimensionless driving field amplitude, and g is the dimensionless diffusion coefficient. Note that ω is no longer explicitly present in the equation.

A. Fokker-Planck equation

Given Eq. (2.2), we can write the Fokker-Planck (Smolukhovskii) [6] equation to describe the probability density $P(\theta,t)$—the probability of the rotor having the position between θ and $\theta+d\theta$ in the time interval from t to $t+dt$:

$$\frac{\partial P}{\partial t}=\frac{\partial}{\partial\theta}(V_\theta P)+\frac{g}{2}\frac{\partial^2 P}{\partial^2\theta}=\hat{L}P\ , \tag{2.3}$$

where $V_\theta\equiv dV/d\theta$ and

$$V(\theta,t)=-\epsilon\cos(\theta)\sin(t) \tag{2.4}$$

is the time-periodic potential well in which the Brownian rotor moves. The operator,

$$\hat{L}=V_{\theta\theta}+V_\theta\frac{\partial}{\partial\theta}+\frac{g}{2}\frac{\partial^2}{\partial\theta^2}\ , \tag{2.5}$$

is a non-self-adjoint operator that governs the dynamical evolution of the Fokker-Planck equation. Because it has time-periodic coefficients, we can use Floquet theory to "solve" the Fokker-Planck equation. For example, we assume the Floquet solution,

$$P(\theta,t)=\phi_\beta(\theta,t)e^{-\Lambda_\beta t}\ , \tag{2.6}$$

where Λ_β is the Floquet eigenvalue and $\phi_\beta(\theta,t)$ is the Floquet eigenstate and is time-periodic $[\phi_\beta(\theta,t)=\phi_\beta(\theta,t+2\pi)]$. After the substitution of Eq. (2.6) into Eq. (2.3), we obtain the eigenvalue equation

$$\Lambda_\beta\phi_\beta(\theta,t)=\left[\frac{\partial}{\partial t}-\hat{L}(\theta,t)\right]\phi_\beta(\theta,t)$$
$$=\hat{W}_{\text{FP}}(\theta,t)\phi_\beta(\theta,t)\ , \tag{2.7}$$

where $\hat{W}_{\text{FP}}(\theta,t)=\partial/\partial t-\hat{L}(\theta,t)$ is the Floquet matrix associated with the Fokker-Planck equation. If the Floquet eigenstates are assumed to be complete, the probability $P(\theta,t)$ takes the form

$$P(\theta,t)=\sum_\beta C_\beta\phi_\beta(\theta,t)e^{-\Lambda_\beta t}\ , \tag{2.8}$$

where the coefficients C_β are determined by the initial condition $P(\theta,0)$. This method of solving the Fokker-Planck equation has been used by several authors [3,4,7,8]. The Floquet eigenvalues Λ_β and eigenvectors $\phi_\beta(\theta,t)$ can be obtained numerically. We now shall show that there is another way of proceeding that allows connection to a Hamiltonian system and as we shall show, gives improved convergence of numerical results.

B. Schrödinger-like equation

Let us now introduce a transformation,

$$P(\theta,t)=\Psi(\theta,t)\exp\left[\frac{-V(\theta,t)}{g}\right]\ . \tag{2.9}$$

After substituting Eq. (2.9) into the Fokker-Planck equation, we obtain what we will refer to as a *Schrödinger-like* equation.

$$-g\frac{\partial\Psi}{\partial t}=-\frac{g^2}{2}\frac{\partial^2\Psi}{\partial^2\theta}+V^*(\theta,t)\Psi=\hat{H}\Psi\ , \tag{2.10}$$

where $V^*(\theta,t)$ is a new effective potential energy,

$$V^*(\theta,t)=-\frac{g}{2}V_{\theta\theta}+\tfrac{1}{2}(V_\theta)^2-V_t$$
$$=\frac{g\epsilon}{2}\cos(\theta)\sin(t)$$
$$-\epsilon\cos(\theta)\cos(t)+\frac{\epsilon^2}{2}\sin^2(\theta)\sin^2(t)\ , \tag{2.11}$$

and

$$\hat{H}=-\frac{g^2}{2}\frac{\partial^2}{\partial^2\theta}+V^*(\theta,t) \tag{2.12}$$

is a self-adjoint Hamiltonian operator which governs the dynamics of the Schrödinger-like equation [Eq. (2.10) is not a Schrödinger equation because it does not have a factor i on the left]. Note that the diffusion coefficient g plays the role of Planck's constant $\hbar$ in the Hamiltonian equation (2.12).

We may also perform the transformation, Eq. (2.9), directly on the Floquet eigenvectors if we let

$$\phi_\beta(\theta,t)=\chi_\beta(\theta,t)\exp\left[\frac{-V(\theta,t)}{g}\right]. \tag{2.13}$$

The Floquet eigenvalue problem now takes the form

$$\Lambda_\beta\chi_\beta(\theta,t)=\left[\frac{\partial}{\partial t}-\hat{H}(\theta,t)\right]\chi_\beta(\theta,t)$$
$$=\hat{W}_{\rm SL}(\theta,t)\chi_\beta(\theta,t)\ , \tag{2.14}$$

where $\hat{W}_{\rm SL}(\theta,t)=\partial/\partial t-\hat{H}(\theta,t)$ is the Floquet operator associated with the Schrödinger-like equation. The Floquet spectrum remains unchanged. The probability now can be written in the form

$$P(\theta,t)=\sum_\beta C_\beta\chi_\beta(\theta,t)\exp\left[\frac{-V(\theta,t)}{g}\right]e^{-\Lambda_\beta t}. \tag{2.15}$$

One can use either Eqs. (2.7) or (2.14) to obtain the Floquet eigenvalues and eigenvectors. We will now compare the results of the two approaches.

C. Numerical results

Since the Floquet eigenstates $\phi_\beta(\theta,t)$ and $\chi_\beta(\theta,t)$ are periodic in angle θ, we can expand them in Fourier series,

$$\phi_\beta(\theta,t)=\frac{1}{\sqrt{2\pi}}a_0^{(\rm FP)}(t)+\frac{1}{\sqrt{\pi}}\sum_{n=1}^{\infty}[a_n^{(\rm FP)}(t)\cos(n\theta)+b_n^{(\rm FP)}(t)\sin(n\theta)]\ , \tag{2.16}$$

and

$$\chi_\beta(\theta,t)=\frac{1}{\sqrt{2\pi}}a_0^{(\rm SL)}(t)+\frac{1}{\sqrt{\pi}}\sum_{n=1}^{\infty}[a_n^{(\rm SL)}(t)\cos(n\theta)+b_n^{(\rm SL)}(t)\sin(n\theta)]\ . \tag{2.17}$$

Because of the symmetry $\hat{L}(\theta,t)=\hat{L}(-\theta,t)$ and $\hat{H}(\theta,t)=\hat{H}(-\theta,t)$, when Eqs. (2.16) and (2.17) are substituted into Eqs. (2.7) and (2.14), respectively, the coefficients $a_n^{(j)}(t)$ and $b_n^{(j)}(t)$ ($j=$FP,SL), decouple. We will only consider the eigenvalue equation involving coefficients $a_n^{(j)}(t)$ because it contains the long time state of the system. The eigenvalue equations then take the form

$$\Lambda a_m^{(j)}(t)=\sum_{n=0}^{\infty}\langle m|\hat{W}_j|n\rangle a_n^{(j)}(t)\ ,$$
$$0\le m\le\infty,\quad j=\text{FP,SL}\ . \tag{2.18}$$

Since the coefficients $a_n^{(\rm FP)}(t)$ and $a_n^{(\rm SL)}(t)$ are time-periodic we can expand them in the Fourier time series,

$$a_n^{(j)}(t)=\frac{1}{\sqrt{2\pi}}\sum_{p=-\infty}^{\infty}\alpha_{n,p}^{(j)}e^{-ipt},\quad j=\text{FP,SL}\ . \tag{2.19}$$

We finally arrive at the eigenvalue equations

$$\Lambda\alpha_{m,q}^{(j)}=\sum_{\substack{n=0\\p=-\infty}}^{\infty}\langle m,q|\hat{W}_j|n,p\rangle\alpha_{n,p}^{(j)}\ ,$$
$$0\le m\le\infty,\quad -\infty\le q\le\infty,\quad j=\text{FP,SL}\ . \tag{2.20}$$

In the formulas above we have used a scalar product defined as follows:

$$\langle n,p|W|m,q\rangle=N(n,m)\int_0^{2\pi}dt\int_0^{2\pi}d\theta\,e^{-ipt}\cos(n\theta)W(\theta,t)\times e^{+iqt}\cos(m\theta)\ , \tag{2.21}$$

where $N(n,m)$ is a normalization factor computed by the rule

$$N(n,m)=\begin{cases}1/(4\pi^2) & \text{for } n=0,\quad m=0\\ 1/(2\sqrt{2}\pi^2) & \text{for } n=0,\quad m\neq0\\ & \text{or } m=0,\quad n\neq0\\ 1/2\pi^2 & \text{for } n\neq0,\quad m\neq0.\end{cases}$$

The Floquet matrices $\langle m,q|\hat{W}_j|n,p\rangle$ are infinite dimensional, complex, and are not self-adjoint. Their entries are given in Appendix A. Notice that this matrix consists of two decoupled blocks. In one block, even combinations $n+p$ are coupled to one another (the even block). In the other block, odd combinations are coupled to one another (the odd block).

To solve the eigenvalue problem numerically one has to truncate the matrix. The spectra for the even block of $\langle m,q|\hat{W}_{\rm SL}|n,p\rangle$ for $0\le m,n\le25,-25\le p,q\le25$, $g=0.2$, and $\epsilon=0.1,0.5,1.0,2.0$ are presented in Fig. 1. The spectra for the even block of $\langle m,q|\hat{W}_{\rm FP}|n,p\rangle$ for $0\le m,n\le25,-25\le p,q\le25$, $g=0.2$, and $\epsilon=0.1,0.5,1.0,2.0$ are presented in Fig. 2. The eigenvalues are complex. The real part gives the decay rates and the imaginary part gives oscillatory (in time) contributions to the probability. Because of the structure of the matrices $\langle m,q|\hat{W}_j|n,p\rangle$, the spectrum has the form $\Lambda=\lambda+ip$, where λ is real and p is an integer (a proof is given in Appendix B). We see that in both cases the lowest value of the real part of the Floquet eigenvalue is zero, corresponding to the long time state. For small ϵ they agree fairly well but become significantly different as ϵ increases.

We believe that the disagreement between the calculated spectra of the Fokker-Planck and the Schrödinger-like Floquet operators can be understood in terms of the transformation [Eqs. (2.6) and (2.13)]. As the parameter ϵ/g increases, the function $\exp[-(\epsilon/g)V(\theta,t)]$ rapidly becomes sharply peaked and becomes very difficult to represent by a finite Fourier series, very much like a δ function. Thus in making the transformation, we have removed a highly singular contribution from the probability and as a result the Fourier expansion of the Schrödinger-like Floquet matrix appears to be much more convergent than the Fokker-Planck Floquet matrix as we shall show in the next section. Furthermore, the fact that the Schrödinger-like Floquet matrix is dominat-

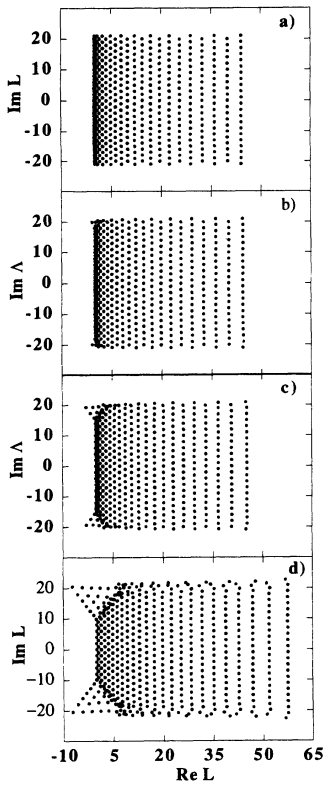

FIG. 1. Floquet spectra of the Schrödinger-like Floquet matrix with imaginary parts plotted against real parts: (a) $g=0.2$, $\epsilon=0.1$; (b) $g=0.2$, $\epsilon=0.5$; (c) $g=0.2$, $\epsilon=1.0$; (d) $g=0.2$, $\epsilon=2.0$.

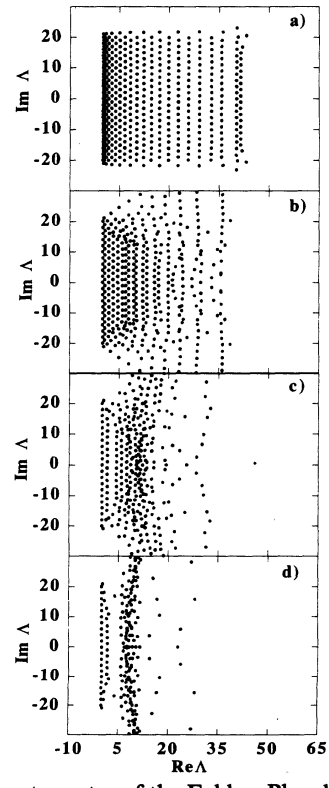

FIG. 2. Floquet spectra of the Fokker-Planck Floquet matrix with imaginary parts plotted against real parts: (a) $g=0.2$, $\epsilon=0.1$; (b) $g=0.2$, $\epsilon=0.5$; (c) $g=0.2$, $\epsilon=1.0$; (d) $g=0.2$, $\epsilon=2.0$.

ed by a Hamiltonian allows us to use ideas from classical and quantum chaos theory to analyze our results. This we will do in subsequent sections.

III. SCHRÖDINGER-LIKE SYSTEM

We now look at the Schrödinger-like system from several points of view to show that it exhibits the manifestations of chaos.

A. Classical system

The Hamiltonian which determines the evolution of the Schrödinger-like system is given in Eq. (2.12). This is simply the quantum Hamiltonian for a rotor in potential field $V^*(\theta,t)$ if we let $g\rightarrow\hbar$. Therefore, we can obtain its classical analog. Let us introduce the angular momentum operator $J=-ig(\partial/\partial\theta)$. Then, the classical Hamiltonian is

$$H=\tfrac{1}{2}J^2+\frac{\epsilon g}{2}\cos(\theta)\sin(t) -\epsilon\cos(\theta)\cos(t)+\frac{\epsilon^2}{2}\sin^2(\theta)\sin^2(t)\ . \tag{3.1}$$

This Hamiltonian contains a number of primary nonlinear resonances. The terms $(\epsilon g/2)\cos(\theta)\sin(t)$ and $\epsilon\cos(\theta)\cos(t)$ give rise to primary resonances [2] at $J=\pm1$. The term $(\epsilon^2/2)\sin^2(\theta)\sin^2(t)$ gives rise to primary resonances at $J=0,\pm1$. These primary resonances can be seen in Fig. 3(a). In addition, the interaction of

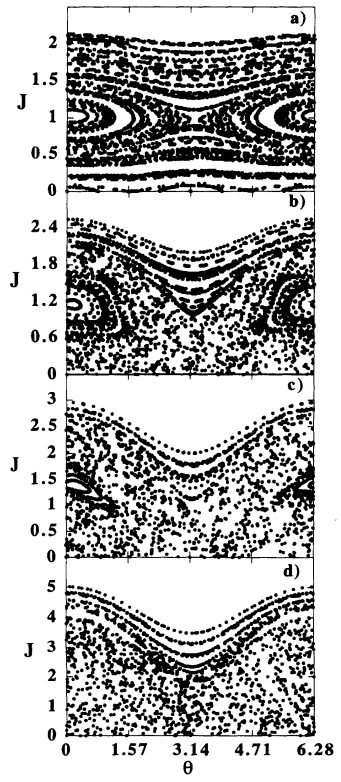

FIG. 3. Strobe plots for the classical system with potential V^*: (a) $g=0.2$, $\epsilon=0.1$; (b) $g=0.2$, $\epsilon=0.5$; (c) $g=0.2$, $\epsilon=1.0$; (d) $g=0.2$, $\epsilon=2.0$.

these primary resonances introduces infinite families of higher-order resonances into the phase space in the neighborhood of the primary resonances. As a result, the system can exhibit a transition to chaos in the region of phase space dominated by the nonlinear resonances.

The equations of motion for the angular momentum J and the angle θ are

$$\frac{dJ}{dt}=\frac{\epsilon g}{2}\sin(\theta)\sin(t)-\epsilon\sin(\theta)\cos(t) -\frac{\epsilon^2}{2}\sin(\theta)\cos(\theta)\sin^2(t) \tag{3.2a}$$

and

$$\frac{d\theta}{dt}=J\ . \tag{3.2b}$$

Strobe plots of the (J,θ) phase space are shown in Fig. 3 for the same values of the diffusion coefficient g and field amplitude ϵ considered in Figs. 1 and 2. At low ϵ the phase space is dominated by KAM surfaces indicating the presence of two global constants of the motion. As the amplitude of the driving field increases the Kolmogorov-Arnold-Moser (KAM) surfaces are destroyed (indicating that one of the constants of motion is destroyed in this region of the phase space by the nonlinear resonances) and chaos appears in the neighborhood of the nonlinear resonances. Before we look at the implications of this transition to chaos for the Brownian rotor, it is of interest to look at the quantum version of the classical system, Eq. (3.1).

B. Quantum system

The quantum version of the classical system, Eq. (3.1), is governed by the Schrödinger equation

$$-i\hbar\frac{\partial\psi}{\partial t}=-\frac{\hbar^2}{2}\frac{\partial^2\psi}{\partial^2\theta}+V^*(\theta,t)\psi\ , \tag{3.3}$$

where $g\rightarrow\hbar$ in Eq. (2.11). Because this partial differential equation has time-periodic coefficients, we again can use Floquet theory to study its time evolution. We assume Floquet solutions of the form

$$\psi(\theta,t)=e^{-i\lambda_\beta t}\pi_\beta(\theta,t) =e^{-i\lambda_\beta t}\frac{1}{\sqrt{2\pi}} \times\sum_{p=-\infty}^{\infty}\frac{1}{\sqrt{2\pi}}e^{-ipt}\left[\frac{1}{\sqrt{2\pi}}\alpha_{0,p} +\frac{1}{\sqrt{\pi}}\sum_{n=1}^{\infty}\alpha_{n,p}\cos(n\theta)\right]\ , \tag{3.4}$$

where λ_β is the Floquet eigenvalue and $\pi_\beta(\theta,t)$ is the time-periodic Floquet eigenvector. Substitution of Eq. (3.4) into Eq. (3.3) yields the eigenvalue problem

$$\lambda\alpha_{m,q}(\theta,t)=\sum_{\substack{n=0\\p=-\infty}}^{\infty}\langle m,q|\hat{M}|n,p\rangle\alpha_{n,p}\ , \qquad 0\le m\le\infty,\quad -\infty\le q\le\infty\ . \tag{3.5}$$

where $\hat{M}=i\hbar(\partial/\partial t)-\hat{H}$ is the Hermitian quantum Floquet Hamiltonian. The Floquet eigenvalues for the quantum system are real.

The onset of chaos in the classical system manifests itself in the quantum system through a change of the Floquet eigenvalue spacing statistics, indicating that a good quantum number (constant of the motion) is being destroyed locally [2,9–11]. For small ϵ, when two good quantum numbers dominate the behavior of the system, the Floquet spectrum forms the purely random distribution of points on a line and the nearest spacing s between Floquet eigenvalues obeys a Poissonian distribution $P(s)\sim e^{-2}$, indicating that there is a high probability of finding very small spacings between eigenvalues. However, as ϵ increases, one of the good quantum numbers is destroyed locally and eigenvalues associated with eigenvectors localized in that region begin to exhibit level repulsion. The nearest-neighbor spacing distribution tends to a Wigner-like distribution $P(s)\sim se^{-s^2}$, with a deficiency of close spacings. This can be seen in Fig. 4, where we show histograms of the level spacings for the

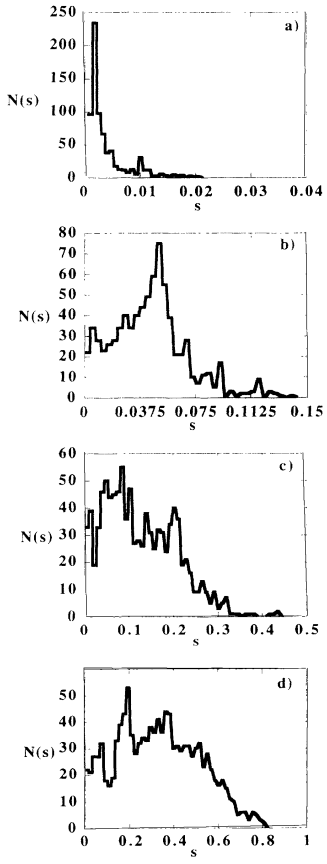

FIG. 4. Level spacing statistics for quantum system with potential V^*: (a) $g=0.2$, $\epsilon=0.1$; (b) $g=0.2$, $\epsilon=0.5$; (c) $g=0.2$, $\epsilon=1.0$; (d) $g=0.2$, $\epsilon=2.0$.

quantum system with $\hbar=0.2$ and $\epsilon=0.1, 0.5, 1.0, 2.0$.

The spectra used to obtain the histograms in Fig. 4 were calculated from the eigenvalue problem, Eq. (3.5), with the truncation of the infinite-dimensional matrix $\langle m,q|\hat{M}|n,p\rangle$ in a manner similar to the cases discussed in Sec. II C. The criterion for the validity of the truncation is the locality of the wave function, i.e., that the entries to the eigenvectors do not run of to the edges. We know that eigenvectors will spread throughout the region dominated by chaos in the underlying classical system. Therefore, the matrix must be large enough to include all eigenstates in the chaotic region. We can easily determine this if we note that the quantum system can be obtained from the classical system by quantizing the angular momentum J. That is, we know that $J=\pm n\hbar$, where n is the quantum number. If we look at Fig. 3(d), we see that the chaotic region extends from $-4\leq J\leq+4$. If $\hbar=0.2$ then there are about 41 spatial modes which lie in the chaotic region of the phase space in Fig. 3(d). Since the Floquet matrix decomposes into four uncoupled blocks, these 41 spatial modes form four independent sets, one containing 11 modes and three containing ten modes. The matrix we use to obtain the Floquet eigenvalues from which we construct the histograms in Fig. 4 is the "even" part of the Floquet matrix obtained using 24 spatial modes ($n=0$ to 23) and 47 time modes ($-23<p<23$). To improve the statistics, for each value of ϵ we also obtained spacings for matrices whose value of ϵ differs by 0.5%. For example, Fig. 4(b) contains spacing for matrices with $\epsilon=0.500, 0.505, 0.495$.

By increasing $\hbar$ and keeping ϵ constant we can indirectly change the number of modes spanning the chaotic region. The size of the chaotic region depends primarily on the value of ϵ, whereas the number of states that sample the chaotic region for a given value of ϵ depends on the size of $\hbar$.

The manifestations of chaos in the quantum system are delayed as compared to the underlying classical system as ϵ is increased. In the classical system, when KAM surfaces are destroyed they form Cantori. As ϵ increases, the gaps in the Cantori grow larger. In the classical system, trajectories can pass through the holes in the Cantori, regardless of how small they are. However, the quantum system cannot "see" the holes (the wave function cannot penetrate them) until they have a size $\hbar$, the size of a quantum state. Thus, in Figs. 3 and 4, level repulsion between Floquet eigenstates lags behind the onset of chaos in the classical phase space as ϵ increases.

IV. STOCHASTIC MANIFESTATIONS OF CHAOS

We now want to show that the transition to chaos in the classical system also manifests itself in the spectrum of the Fokker-Planck equation and in the stochastic properties of the driven Brownian rotor. In practice, we can obtain this spectrum from either the Fokker-Planck Floquet matrix or from the Schrödinger-like Floquet matrix. As we indicated in Sec. II, the Schrödinger-like Floquet matrix, when performing actual numerical calculations, gives more accurate results.

We have found that the behavior of the Schrödinger-like spectrum can be understood from the behavior of the underlying classical Hamiltonian system. Let us note that for small ϵ, $\mathrm{Re}\Lambda_\beta\approx J^2=(ng)^2$, while $\mathrm{Im}\Lambda_\beta=p$ (p is an integer). Thus, the smallest decay rates (those determining the long-time transient behavior) are directly affected by the chaotic region of the classical system and we expect them to exhibit level repulsion as ϵ increases and chaos sets in. In order to study this effect, in Fig. 5 we plot the difference between each rate of decay for a given ϵ and the corresponding rate for $\epsilon=0.1$, as a function of ϵ. Thus Fig. 5 illustrates exactly how much each consecutive level was shifted from its value at $\epsilon=0.1$ as the chaos sets in. Note that relatively high decay rates (levels) do not exhibit mutual level repulsion, while the low ones do. Note also that the number of mutually repelling levels increase with ϵ. This increase happens at the same ranges of ϵ as the change in statistics in Fig. 4 and the onset of chaos in Fig. 3. For example, the strobe plot in Fig. 3(d), where $\epsilon=2.0$ and $g=0.2$, about ten states sample the chaotic region between $J=-4.0$ and 4.0 since we are only looking at the spectrum of the even block of Eq. (2.14). Of these ten states, only about six are completely in the chaotic region. If we look at Fig. 5, we see that only six states repel one another.

The effect of the transition to chaos in the classical system can also be seen rather dramatically in the first-passage time. In Ref. [4], a mean-first-passage time [12] for a Brownian rotor moving in the potential $V(\theta,t)=-2\epsilon_0\cos(\theta)\cos(\omega_0 t)$ was computed. In that paper, the dimensionless amplitude ϵ_0 and dimensionless frequency ω_0, were used as parameters, and the diffusion coefficient was taken to be 1. The Fokker-Planck equation for the system in Ref. [4] can be written in the form shown in Eq. (2.3) by rescaling the time and taking $\epsilon_0=\epsilon/g$ and $\omega_0=2/g$. The classical Hamiltonian underlying the Brownian motion in Ref. [4] is identical to ours if $g=2/\omega_0$ and $\epsilon=2\epsilon_0/\omega_0$, except that the resonances will be phase shifted relative to ours. The extent of the chaotic region as a function of the parameters will not change. Therefore, we can relate the mean-first-passage-time results of Ref. [4] to the extent of chaos in our Hamiltonian system.

In Ref. [4], the mean-first-passage time for the Brownian rotor was computed for the case when the rotor is started at $\theta=\pi/2$ and absorbing boundaries are placed at

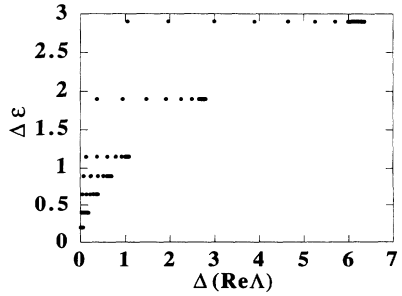

FIG. 5. Shift in each decay rate ($\mathrm{Re}\Lambda$) with increasing ϵ, measured with respect to its value when $\epsilon=0.1$. In all cases $g=0.2$.

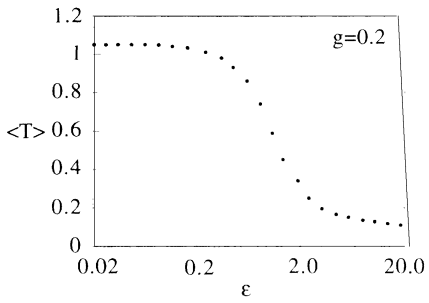

FIG. 6. A plot of a mean-first-passage time for the Brownian rotor as a function of ϵ for $g=0.2$ (based on data from Ref. [4]).

$\theta=0$ and $\theta=\pi$. The data from Ref. [4] are reproduced in Figs. 6 and 7, but plotted as a function of g and ϵ. It is important to note that the behavior of the mean-first-passage time is largely determined by the behavior of the lowest decay rates and varies as the inverse of the lowest decay rates. Since the lowest decay rates $\mathrm{Re}\Lambda_\beta$ repel and increase in value when chaos sets in our underlying Hamiltonian, the mean-first-passage time should decrease when chaos sets in.

Let us first consider Fig. 6, which is a plot of the mean-first-passage time for $g=0.2$ as a function of ϵ. We can therefore compare it to the strobe plots in Fig. 3. We see that for $\epsilon=0.1$ there is no chaos and the mean-first-passage time has its largest value. However, as ϵ increases there is a perfect correspondence between the onset of chaos and the drop in the mean-first-passage time due to level repulsion.

Let us next look at Fig. 8, which is a sequence of strobe plots for $\epsilon=10g$ and $g=0.02$, $g=0.1$, $g=0.2$, and $g=2.0$. These correspond to points on the mean-first-passage-time plot of Fig. 7. Note that for $g=0.002$ and $\epsilon=0.2$ [cf. Fig. (8a)] there is almost no chaos (the neighborhood of $J=0$ is regular) and a large mean-first-passage time. When $g=0.1$ and $\epsilon=1.0$, chaos has set in and the mean-first-passage time has dropped. For $g=0.2$ and $\epsilon=2.0$ there is an even more chaotic area, and the mean-first-passage time has dropped still further. However, for $g=2.0$ and $\epsilon=20.0$ the mean-first-passage time starts to rise even though a large region in the neighborhood of $J=0$ is chaotic. This can be understood if we note that the size of the states is now increasing faster than the area of the chaotic region. The size of the chaotic region increases as $\sqrt{\epsilon}$. The number of states that sample that region goes as $n\approx\sqrt{\epsilon}/g$. The mean-first-passage-time points in Fig. 7 lie along a curve $\epsilon=10g$. Thus, the number of states that sample the chaotic region vary as $n\approx 1/\sqrt{g}$. The rise in the mean-first-passage-time curve as g increases occurs because the stochastic states "see" less and less of the chaotic region.

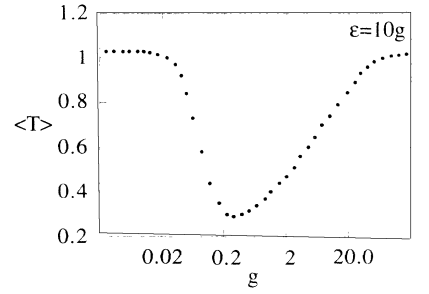

FIG. 7. A plot of a mean-first-passage time for the Brownian rotor for $\epsilon=10g$ as a function of g (based on data from Ref. [4]).

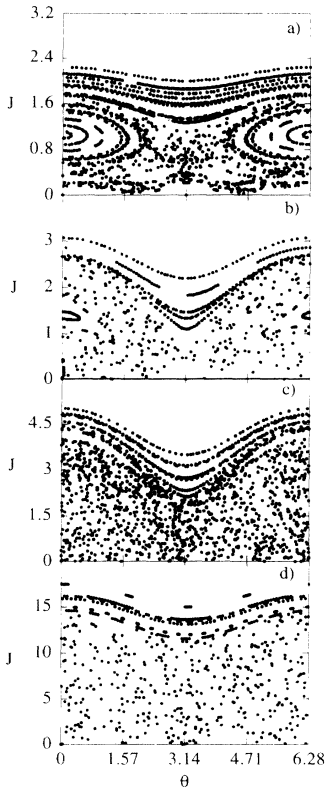

FIG. 8. Strobe plots for the classical system with potential V^*: (a) $g=0.02$, $\epsilon=0.2$; (b) $g=0.1$, $\epsilon=1.0$; (c) $g=0.2$, $\epsilon=2.0$; (d) $g=2.0$, $\epsilon=20$.

V. CONCLUSIONS

Reichl, Chen, and Millonas [3,4] have shown that level repulsion exists in the spectrum of the Fokker-Planck equation for a model similar to that considered here. They examined the Fokker-Planck Floquet spectrum for both an integrable Fokker-Planck equation and a nonintegrable one such as that considered here. They found a distinct difference in the spectral statistics of the two systems. The integrable system had a large number of close spacings. The nonintegrable system showed level repulsion. What is amazing is that these differences showed up in the Fokker-Planck spectrum, even though this widely used method of finding the Floquet spectrum appears not to be as accurate as the method we have introduced in this paper. The results we have obtained here strongly

support the conclusions of that earlier work and the work of Millonas and Reichl [1] for a time-independent system. More specifically, we have found that, for Brownian particles moving in time-independent or time-periodic potential wells in the presence of white noise, a transition in the statistical properties of the decay rates occurs when an underlying Hamiltonian system exhibits a transition to chaos. Furthermore, the decay rates affected by the chaotic region generally repel and become larger, thus affecting the rate of decay of the Brownian particle, the way in which it is distributed as it decays, and other stochastic quantities such as the mean-first-passage time. What is most striking is that in many respects, this stochastic system behaves as if it were "quantized."

ACKNOWLEDGMENTS

The authors wish to thank the Welch Foundation for partial support of this work on Grant No. 1051. The authors also wish to thank David Leonard for helpful discussions, and the University of Texas System Center for High Performance Computing for use of their facilities.

APPENDIX A

The matrix elements of the operator $\hat{W}_{\rm FP}$ in Eq. (2.20) are the following:

(i) For $m=0$, $\langle m,q|\hat{W}_{\rm FP}|n,p\rangle = ip\delta_{n,0}\delta_{p,q}$.

(ii) For $m\neq 0$,

$$\begin{aligned}\langle m,q|\hat{W}_{\rm FP}|n,p\rangle =& \frac{g}{2}n^2\delta_{n,m}\delta_{p,q}-\frac{\epsilon^2}{2\sqrt{2g}}(\delta_{p,q}-\tfrac{1}{2}\delta_{p+2,q}-\tfrac{1}{2}\delta_{p-2,q})\delta_{m,2}\delta_{n,0}-\frac{\epsilon}{2\sqrt{2g}}(\delta_{p+1,q}+\delta_{p-1,q})\delta_{m,1}\delta_{n,0}\\
&-\frac{\epsilon^2}{4g}(\delta_{n+2,m}+\delta_{n-2,m}+\delta_{n-2,-m})(\delta_{p,q}-\tfrac{1}{2}\delta_{p+2,q}-\tfrac{1}{2}\delta_{p-2,q})\\
&\times(1-\delta_{n,0})-\frac{\epsilon}{4g}(\delta_{n+1,m}+\delta_{n-1,m})(\delta_{p+1,q}+\delta_{p-1,q})(1-\delta_{n,0})\\
&+\frac{\epsilon^2}{8g}(\delta_{n-2,m}-\delta_{n+2,m}+\delta_{n-2,-m})(\delta_{p,q}-\tfrac{1}{2}\delta_{p+2,q}-\tfrac{1}{2}\delta_{p-2,q})n\\
&\times(1-\delta_{n,0})+\frac{\epsilon}{4g}(\delta_{n-1,m}-\delta_{n+1,m})(\delta_{p+1,q}+\delta_{p-1,q})n(1-\delta_{n,0})\\
&+ip\delta_{p,q}\delta_{n,m}-i\frac{\epsilon}{4\sqrt{2}}(\delta_{p+1,q}-\delta_{p-1,q})\delta_{m,1}\delta_{n,0}\\
&-i\frac{\epsilon}{8}(\delta_{n-1,m}-\delta_{n+1,m})(\delta_{p+1,q}-\delta_{p-1,q})(1-\delta_{n,0})\\
&+\frac{\epsilon}{8}(\delta_{n-1,m}-\delta_{n+1,m})(\delta_{p+1,q}+\delta_{p-1,q})n(1-\delta_{n,0}).\end{aligned}$$

The matrix elements of operator $\hat{W}_{\rm SL}$ in Eq. (2.20) are the following:

(i) For $m=0$,

$$\begin{aligned}\langle m,q|\hat{W}_{\rm SL}|n,p\rangle =& \frac{\epsilon^2}{8g}\delta_{p,q}\delta_{n,0}-\frac{\epsilon^2}{16g}(\delta_{p+2,q}+\delta_{p-2,q})\delta_{n,0}-\frac{\epsilon}{8\sqrt{2g}}\delta_{p,q}\delta_{n,2}+\frac{\epsilon^2}{16\sqrt{2g}}(\delta_{p+2,q}+\delta_{p-2,q})\delta_{n,2}\\
&-\frac{\epsilon}{2\sqrt{2g}}(\delta_{p+1,q}+\delta_{p-1,q})\delta_{n,1}+ip\delta_{n,0}\delta_{p,q}-\frac{i\epsilon}{4\sqrt{2}}(\delta_{p+1,q}-\delta_{p-1,q})\delta_{n,1}.\end{aligned}$$

(ii) For $m\neq 0$,

$$\begin{aligned}\langle m,q|\hat{W}_{\rm SL}|n,p\rangle =& \frac{g}{2}n^2\delta_{p,q}\delta_{m,n}-\frac{\epsilon^2}{8\sqrt{2g}}\delta_{m,2}\delta_{n,0}\delta_{p,q}+\frac{\epsilon^2}{16\sqrt{2g}}(\delta_{p+2,q}+\delta_{p-2,q})\delta_{m,2}\delta_{n,0}\\
&-\frac{\epsilon}{2\sqrt{2g}}(\delta_{p+1,q}+\delta_{p-1,q})\delta_{m,1}\delta_{n,0}+\frac{\epsilon^2}{8g}\delta_{m,n}\delta_{p,q}-\frac{\epsilon^2}{16g}(\delta_{p+2,q}+\delta_{p-2,q})\delta_{n,m}\\
&-\frac{\epsilon^2}{16g}(\delta_{n+2,m}+\delta_{n-2,m}+\delta_{n-2,-m})\delta_{p,q}(1-\delta_{n,0})\\
&+\frac{\epsilon^2}{32g}(\delta_{p+2,q}+\delta_{p-2,q})(\delta_{n+2,m}+\delta_{n-2,m}+\delta_{n-2,-m})(1-\delta_{n,0})\\
&-\frac{\epsilon}{4g}(\delta_{n+1,m}+\delta_{n-1,m})(\delta_{p+1,q}+\delta_{p-1,q})(1-\delta_{n,0})+ip\delta_{p,q}\delta_{m,n}\\
&+\frac{i\epsilon}{4\sqrt{2}}(\delta_{p+1,q}-\delta_{p-1,q})\delta_{n,0}\delta_{m,1}-\frac{i\epsilon}{8}(\delta_{p+1,q}-\delta_{p-1,q})(\delta_{n+1,m}+\delta_{n-1,m})(1-\delta_{n,0}).\end{aligned}$$

For the numerical formulation of eigenvalue problems these expressions are to be substituted in Eq. (2.20) with $-N \leq p \leq N$ and $0 \leq n \leq N$, where N is the desired number of modes in the Fourier expansion.

APPENDIX B

Examination of the Floquet matrices $\langle m,q|W_j|n,p\rangle$ in Appendix A shows the general structure of their spectra. Let us translate the indices q and p so that $q \rightarrow q+p_0$ and $p \rightarrow p+p_0$. We find

$$\langle m,q+p_0|W_j|n,p+p_0\rangle = \langle m,q|W_j|n,p\rangle + ip_0\delta_{p,q}\delta_{n,m} .$$

Thus, the matrix $\langle m,q|W_j|n,p\rangle$ has a periodic block structure, except that the imaginary term on the diagonal of each block changes by an integer value as we move from one block to another. (This same property has been pointed out by Shirley [13] for the quantum Floquet matrix $\langle m,q|M|n,p\rangle$.) The secular equation which determines the spectrum of the Floquet matrix is

$$\det(W_j - \Lambda I) = 0 ,$$

where I is the unit matrix. Now let $\Lambda \rightarrow \Lambda + ip_0$. Then,

$$\det[W_j - (\Lambda + ip_0)I] = \det(W_j + ip_0 I - \Lambda I) = \det(W_j - \Lambda I) = 0 .$$

Thus, if Λ is an eigenvalue, so is $\Lambda + ip_0$, and the spectrum must have the rigid lattice structure seen in Fig. 1.

[1] M. Millonas and L. E. Reichl, Phys. Rev. Lett. **68**, 3125 (1992).

[2] L. E. Reichl, *The Transition to Chaos In Conservative Classical Systems: Quantum Manifestations* (Springer-Verlag, New York, 1992).

[3] L. E. Reichl, Z-Y. Chen, and M. Millonas, Phys. Rev. Lett. **63**, 2013 (1989).

[4] L. E. Reichl, Z-Y. Chen, and M. Millonas, Phys. Rev. A **41**, 1874 (1990).

[5] Z-Y. Chen, Phys. Rev. A **42**, 5837 (1990).

[6] H. Risken, *The Fokker-Planck Equation* (Springer-Verlag, Berlin, 1984).

[7] H. Gang, G. Nicolis, and C. Nicolis, Phys. Rev. A **42**, 2030 (1990).

[8] P. Jung and P. Hanggi, Europhys. Lett. **8**, 505 (1989).

[9] M. L. Mehta, *Random Matrices and the Statistical Theory of Energy Levels* (Academic, New York, 1967).

[10] F. Haake, *Quantum Signature of Chaos* (Springer-Verlag, Berlin, 1990).

[11] M. V. Berry, *Quantum Chaos and Statistical Nuclear Physics,* edited by T. H. Seligman and H. Nishioka, Lecture Notes in Physics Vol. 263 (Springer-Verlag, Berlin, 1986).

[12] G. H. Weiss, Adv. Chem. Phys. **XIII**, 1 (1967).

[13] J. H. Shirley, Ph.D. thesis, California Institute of Technology, 1963 (unpublished).